Eikonal Methods for Complex Anisotropic Ray Tracing

Aaron Wienkers
Caleb Levy
Chung-Hsiang Jiang
Philip Marcus

Abstract

Energy transport to Baroclinic critical layers by internal gravity waves was proposed as a means of lattice replication of *Zombie Vortices* evidenced in simulations near Baroclinic critical layers. A discrete Eikonal solution for stratified, shearing, and rotating systems was developed to verify the energy path to these critical layers by tracing internal wave ray paths. A methodology for performing complex-valued dispersion ray tracing to determine wave trajectory, amplitude, and energy evolution using the Hamiltonian set is also presented. Methods for interpreting the quasi-autonomous complex dispersion relation for three-dimensional inertial and internal gravity waves are posed and shown to be consistent for real-valued cases.

Introduction

Solutions are known and well studied for systems with shear and stratification in the same direction as manifest in many geophysical flows. However, in astrophysical disks, the shear and stratification are often in orthogonal directions, breaking horizontal isotropy. Numerical simulations have revealed a self-replicating lattice of vortices, referred to as *Zombie Vortices* (*Marcus*, et al 2013). The evolution of these stable vortices have been examined in spectral simulations, where thin arms were noticed extending to each consecutive critical layer. These observed arms are thought to be, in addition to the internal gravity wave ray path, the path of the energy flux protruding from each vortex, transporting energy to each critical layer (*Pei* 2013, in preparation).

To verify this hypothesis, the Eikonal ray equations must be solved for the linearly stratified, Keplerian (anticyclonic) shearing, and rotating flow. Analytical solutions for more elementary cases are presented in the leading half of this paper to develop a structure for interpreting the impending complex-valued dispersion relation of the more complicated system described above. In the simplest cases, the Eikonal solution gives a constant propagation angle. In the final case, an analytical solution is not feasible, and thus a quasi-autonomous functional form of the eigenmodes were used to derive a now complex-valued dispersion relation. Solution of the ray equations was then found by numerical solution of the set of partial differential equations.

Solving the Eikonal set forcing a real dispersion relationship is well studied, and this is a good approximation for cases of a slowly shearing system such as that found in the atmosphere (*Dieminger, et al*, 1996) or in oceanographic applications (*Olbers*, 1981 and *Kalashnik*, 2013) where shear is small compared to the Brunt-Väisälä frequency, rotation, and perturbation frequencies. In Keplerian shear, this assumption cannot be made, and shear remains in the dispersion relationship.

The generalized governing equations are the Boussinesq set,

$$\begin{aligned} \frac{\partial \boldsymbol{U}}{\partial t} &= -\left(\boldsymbol{U}\cdot\nabla\right)\boldsymbol{U} - \frac{\nabla p}{\rho_0} + \boldsymbol{U}\times f\hat{\mathbf{z}} - \frac{\rho}{\rho_0}g\hat{\mathbf{z}} \\ \nabla\cdot\boldsymbol{U} &= 0 \\ \frac{\partial \rho}{\partial t} &= -\left(\boldsymbol{U}\cdot\nabla\right)\rho \end{aligned} \tag{1}$$

where $\boldsymbol{U} = u\hat{\mathbf{x}} + v\hat{\mathbf{y}} + w\hat{\mathbf{z}}$ is the total velocity field, f is the Coriolis parameter, and the Boussinesq approximation assumes the density variations are negligible except in the buoyancy term.

Decomposing the equations of motion in accord with perturbation methods using "barred" background quantities and small order "primed" perturbation quantities, and then linearizing the result about the equilibrium solution gives the perturbation form which has general normal modes of the form $\xi = \hat{\xi}(\boldsymbol{x},t)e^{i(k_x x + k_y y + k_z z - \omega t)}$. In the linearized result, $\bar{\rho}(z)$ is implicitly defined by the Brunt-Väisälä frequency $N^2 \equiv -\frac{g}{\rho_0}\frac{d\bar{\rho}}{dz}$.

The generalized Eikonal Ray equations are given as (*Lighthill*, 1978)

$$\begin{aligned} \frac{d\boldsymbol{k}}{dt} &= -\nabla_x\Omega - k_i\frac{\partial U_i}{\partial \boldsymbol{x}} = -\nabla_x\omega \\ \frac{d\boldsymbol{x}}{dt} &= \boldsymbol{c}_g + \bar{\boldsymbol{U}} = \nabla_k\omega + \bar{\boldsymbol{U}} \end{aligned} \tag{2}$$

where $\Omega = \omega - \bar{\boldsymbol{U}}\cdot\boldsymbol{k}$ is the extrinsic, or relative frequency, and where the substantial derivatives are evaluated along the ray path, with the group velocity. Similar to the Hamiltonian equations, the first equation governs wave refraction, whereas the latter describes the group velocity. In the Lagrangian frame with no background shear, and using the ray equations above, a useful result is obtained:

$$\frac{d\omega}{dt} = \frac{\partial\omega}{\partial t} = 0$$

since the dispersion relation takes the form $\omega = f(\boldsymbol{k},\boldsymbol{x})$ for the steady systems of interest. Therefore, the wave frequency is identically the perturbation frequency, which remains constant while following a traced ray.

For completeness, and to gain an intuition into the complex-valued cases, the dispersion relation, and direction of energy propagation, are derived and presented below, both in non-shearing and shearing flows:

1. No shear (i.e. $\bar{\boldsymbol{U}} = 0$).
   (a) $f = const$ and $N = const$
   (b) $f = const$ and $N(z)$, using WKB approximation
2. With shear (i.e. $\bar{\boldsymbol{u}} = \sigma y\hat{\mathbf{x}}$)
   (a) $f = const$, $N = const$ and $k_x = 0$
   (b) $f = const$, $N(z)$ and $k_x = 0$

1 No Shear

The simplest internal inertia-gravity wave is a plain Poincaré wave, where the Coriolis force is sufficient to force dispersion when $f \sim kc$ (*Gill*, 1982). Linearizing the equations of motion about $\bar{\boldsymbol{U}} = 0$ so that $\boldsymbol{U} = \boldsymbol{U}' = u'\hat{\mathbf{x}} + v'\hat{\mathbf{y}} + w'\hat{\mathbf{z}}$ and using $\rho = \bar{\rho}(z) + \rho'(\boldsymbol{x}, t)$, $p = \bar{p} + p'$, the advection term then drops out, leaving

$$\frac{\partial \boldsymbol{U}'}{\partial t} = -\frac{\nabla p'}{\rho_0} + \boldsymbol{U}' \times f\hat{\mathbf{z}} - \frac{\rho'}{\rho_0} g\hat{\mathbf{z}}. \tag{3}$$

Utilizing the definition of the Brunt-Väisälä frequency, N, the density equation becomes

$$\frac{\partial \rho'}{\partial t} = -w' \frac{\partial \bar{\rho}}{\partial z} = \frac{\rho_0 w' N^2}{g}. \tag{4}$$

1.1 Constant Frequencies

Since Equations 3 and 4 are autonomous in x, y, z, and t and the system is unbounded, the eigenmodes take the form

$$\xi = \hat{\xi} e^{i(k_x x + k_y y + k_z z - \omega t)}$$

which holds whenever N and f are constant. The x-y plane is isotropic for $\sigma = 0$, thus k_y can be absorbed into k_x, to simplify this to a 2-D problem. Thus Equations 3 and 4, along with continuity can be written using the normal modes as

$$\begin{aligned} -i\omega\hat{u}' &= -\frac{ik_x}{\rho_0}\hat{p}' + f\hat{v}' \\ -i\omega\hat{w}' &= -\frac{ik_z}{\rho_0}\hat{p}' - \frac{\hat{\rho}' g}{\rho_0} \\ -i\omega\hat{v}' &= -f\hat{u}' \\ ik_x\hat{u}' + ik_z\hat{w}' &= 0 \\ -i\omega\hat{\rho}' &= \frac{\rho_0 N^2}{g}\hat{w}'. \end{aligned} \tag{5}$$

Solving this system with constant N and $f = 0$ gives the dispersion relation $-\frac{k_z^2}{k^2} = \frac{\omega^2 + N^2}{N^2}$ where $k = |\boldsymbol{k}| = \sqrt{k_x^2 + k_y^2 + k_z^2}$. Defining $\sin\theta = \frac{k_z}{k}$, the angle between the perturbation and propatation direction, this relation becomes

$$\frac{\omega}{N} = \cos\theta. \tag{6}$$

Note that as $\omega \to N$, $\theta \to 0$, i.e. the wavevector $\boldsymbol{k}$ is pointing along the x-axis, and the wave's direction (group velocity), is vertical. If $\omega \ll N$, then $\theta \to \frac{\pi}{2}$ and the wave propagates horizontally.

If f is now a constant and $N = 0$, using a similar procedure the dispersion relation becomes $1 - \frac{f^2}{N^2} = -\cot^2\theta$, or

$$\sin\theta = \pm\frac{\omega}{f}. \tag{7}$$

Note that as $\omega \to f$, $\theta \to \frac{\pi}{2}$ (i.e. the wave travels horizontally) and as $\omega \ll f$, $\theta \to 0$ and the wave propagates vertically.

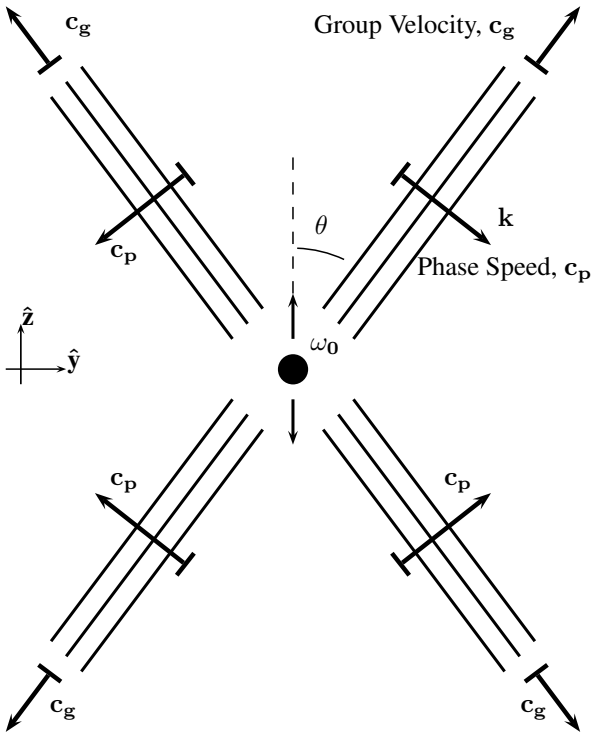

Figure 1: Diagram detailing group and phase velocity vectors relative to the wavevector.

In general, for constant values of N and f, the dispersion relation becomes

$$\omega^2 = N^2 \cos^2\theta + f^2 \sin^2\theta = N^2 \frac{k_x^2}{k_x^2 + k_z^2} + f^2 \frac{k_z^2}{k_x^2 + k_z^2} \tag{8}$$

which can also be written as $\frac{k_x^2}{k_z^2} = \frac{\omega^2 - f^2}{N^2 - \omega^2}$.

In either case, the phase and group velocities are given, respectively, by

$$\boldsymbol{c}_p = \frac{\omega}{k^2}\boldsymbol{k}, \qquad\qquad \boldsymbol{c}_g = \frac{\partial\omega}{\partial k_x}\hat{\mathbf{x}} + \frac{\partial\omega}{\partial k_y}\hat{\mathbf{y}} + \frac{\partial\omega}{\partial k_z}\hat{\mathbf{z}}.$$

The phase and group velocities of the internal waves in the first case then can be shown to be

$$\begin{aligned}
\boldsymbol{c}_p &= \frac{Nk_x}{k^3}\left(k_x\hat{\mathbf{x}} + k_z\hat{\mathbf{z}}\right) \\
\boldsymbol{c}_g &= \frac{Nk - Nk_x^2/k}{k^2}\hat{\mathbf{x}} - \frac{Nk_xk_z}{k^3}\hat{\mathbf{z}} \\
&= \frac{Nk_z}{k^3}\left(k_z\hat{\mathbf{x}} - k_x\hat{\mathbf{z}}\right).
\end{aligned}$$

It is apparent that $\boldsymbol{c}_p \cdot \boldsymbol{c}_g = 0$, verifying that the group and phase velocities are orthogonal. Similarly

in the second case,

$$\begin{aligned}\boldsymbol{c}_p &= \frac{fk_z}{k^3}\left(k_x\hat{\mathbf{x}} + k_z\hat{\mathbf{z}}\right)\\ \boldsymbol{c}_g &= -\frac{fk_zk_x}{k^3}\hat{\mathbf{x}} + \frac{fk - fk_z^2/k}{k^2}\hat{\mathbf{z}}\\ &= \frac{fk_x}{k^3}\left(-k_z\hat{\mathbf{x}} + k_x\hat{\mathbf{z}}\right).\end{aligned}$$

Again it is apparent that $\boldsymbol{c}_p \cdot \boldsymbol{c}_g = 0$. In the final constant property case where the dispersion relation, (8), is rewritten as $\omega^2 = \frac{1}{k^2}\left(N^2k_x^2 + f^2k_z^2\right)$ the phase and group velocities become

$$\begin{aligned}\boldsymbol{c}_p &= \frac{\omega}{k^2}\left(k_x\hat{\mathbf{x}} + k_z\hat{\mathbf{z}}\right)\\ \boldsymbol{c}_g &= \frac{k_x}{\omega k^2}\left(N^2 - \omega^2\right)\hat{\mathbf{x}} + \frac{k_z}{\omega k^2}\left(f^2 - \omega^2\right)\hat{\mathbf{z}} = \frac{1}{\omega k^2}\left[\boldsymbol{k}\left(N^2 - \omega^2\right) - k_z\left(N^2 - f^2\right)\hat{\mathbf{z}}\right]\\ &= \frac{k_xk_z}{\omega k^4}\left(N^2 - f^2\right)\left(k_z\hat{\mathbf{x}} - k_x\hat{\mathbf{z}}\right).\end{aligned} \tag{9}$$

Again $\boldsymbol{c}_p \cdot \boldsymbol{c}_g = k_x^2\left(N^2 - \omega^2\right) + k_z^2\left(f^2 - \omega^2\right) = -k^2\omega^2 + \omega^2k^2 = 0$. Examining the consequences of this result, and given that $N > f > \omega$, it is shown that as $\theta \to 0, \frac{\pi}{2}$ then $\boldsymbol{c}_g \to 0$.

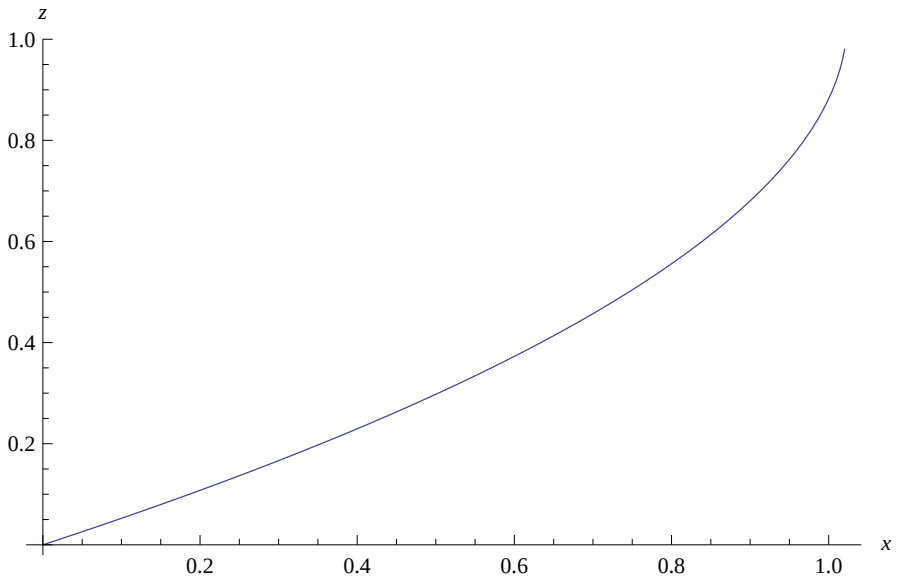

Figure 2: Wave packet trajectory for variably stratified flow, $\omega = 2f = N_0$ and $N(z) = N_0(1 - z/5)$, with x-y isotropy.

1.2 Variably Stratified Background

With variable $N(z)$, the periodic normal modes for the governing equations, (1), are no longer autonomous in z, and become

$$\xi = \hat{\xi}(z)\, e^{i(k_x x + k_y y - \omega t)}.$$

Writing the governing equations using these normal modes gives the coupled system of five differential equations:

$$\begin{aligned} -i\omega\hat{u}' &= -\frac{ik_x}{\rho_0}\hat{p}' + f\hat{v}' \\ -i\omega\hat{v}' &= -f\hat{u}' \\ -i\omega\hat{w}' &= -\frac{1}{\rho_0}\frac{d\hat{p}'}{dz} - \frac{g\hat{\rho}'}{\rho_0} \\ -i\omega\hat{\rho}' = -\frac{d\bar{\rho}}{dz}\hat{w}' &= \frac{\rho_0}{g}N^2(z)\,\hat{w}' \\ -ik_x\hat{u}' + \frac{d\hat{w}'}{dz} &= 0. \end{aligned} \tag{10}$$

Reducing this system to a single second order differential equation gives

$$\frac{d^2\hat{w}'}{dz^2} + k_x^2\left[\frac{N^2(z)-\omega^2}{\omega^2-f^2}\right]\hat{w}' = 0.$$

Approximating the solution of this differential equation using the WKB method as described by Mathews and Walker (1973) will allow solution for the dispersion relation.

Defining $R^2(z) = k_x^2\left[\frac{N^2(z)-\omega^2}{\omega^2-f^2}\right]$ the differential equation is simplified as

$$\frac{d^2\hat{w}'}{dz^2} + R^2\hat{w}' = 0$$

which indicates that a stable solution exists only when $R^2 > 0$, or

$$N > \omega > f.$$

When this condition is not satisfied, the exponentially decreasing field variables given by the solution of the differential equation is an evanescent mode, which by energy conservation arguments, wave reflection must occur. Mathews and Walker propose a solution to this differential equation in the form $\hat{w}' = A(z)\,e^{i\phi(z)}$. Their WKB solution is given as

$$\hat{w}' = \frac{A_0}{\sqrt{R}}e^{\pm i\int R dz}. \tag{11}$$

By term matching with the oscillatory term of the eigenmodes of this solution, $R^2(z)$ is analogous to $k_z^2(z)$, so the dispersion relation is

$$k_z^2(z) = k_x^2\left[\frac{N^2(z)-\omega^2}{\omega^2-f^2}\right] \qquad \text{given } \frac{\omega}{N\sqrt{dN/dz}} \ll 1.$$

Using this result along with (9), integrating in x and z for each parametric component in t, the wave path becomes

$$x = \frac{\left[N^2(z)-\omega^2\right]}{\sqrt{\omega^2-f^2}}\frac{\ln\left(N(z)+\sqrt{N^2(z)-\omega^2}\right)}{dN/dz} + c(z)$$

$$\text{where } c(z) = \frac{\ln\left(N(0)+\sqrt{N^2(0)-\omega^2}\right)}{dN/dz\sqrt{\omega^2-f^2}}\left[N^2(z)-\omega^2\right]$$

using the boundary condition, $\boldsymbol{x}(t=0) = \mathbf{0}$.

2 Constant Shear

Adding to the domain a constant shear, $\bar{\boldsymbol{U}} = \sigma y \hat{\mathbf{x}}$, into the Boussinesq set, 1, linearizing about $\bar{\boldsymbol{U}}$ and dropping second order terms, the linearized equations of motion become

$$\begin{aligned} \frac{\partial \boldsymbol{U}'}{\partial t} = -\left(\bar{\boldsymbol{U}} \cdot \nabla\right) \boldsymbol{U}' - \left(\boldsymbol{U}' \cdot \nabla \bar{\boldsymbol{U}}\right) - \frac{\nabla p'}{\rho_0} + \boldsymbol{U}' \times f\hat{\mathbf{z}} - \frac{\rho'}{\rho_0} g\hat{\mathbf{z}} \\ \nabla \cdot \boldsymbol{U}' = 0 \\ \frac{\partial \rho'}{\partial t} = -\bar{u}\frac{\partial \rho'}{\partial x} + w' \frac{\rho_0 N^2}{g}. \end{aligned} \tag{12}$$

2.1 Constant N, $k_x = 0$

With a spatially varying background flow, the described system is not autonomous in y, so the eigenmodes take the form

$$\xi = \hat{\xi}(y)\, e^{i(k_x x + k_z z - \omega t)}.$$

Additionally, the horizontal isotropy is broken with the addition of shear. Rewriting this system using the normal modes, it becomes

$$\begin{aligned} -i\omega\hat{u}' = -ik_x\bar{U}\hat{u}' - \sigma\hat{v}' - \frac{ik_x}{\rho_0}\hat{p}' + \hat{v}' f \\ -i\omega\hat{v}' = -ik_x\bar{U}\hat{v}' - \frac{1}{\rho_0}\frac{d\hat{p}'}{dy} - \hat{u}' f \\ -i\omega\hat{w}' = -ik_x\bar{U}\hat{w}' - \frac{ik_z}{\rho_0}\hat{p}' - \frac{g}{\rho_0}\hat{\rho}' \\ ik_x\hat{u}' + \frac{d\hat{v}'}{dy} + ik_z\hat{w}' = 0 \\ -i\omega\hat{\rho}' = -ik_x\bar{U}\hat{\rho}' + \hat{w}'\frac{\rho_0 N^2}{g}. \end{aligned} \tag{13}$$

Again, each hatted term is a function now of y. In order to make the relationships between the fields in question more apparent, the shearing-sheet transformation is adopted to force autonomy in the y direction by exploiting periodicity in $\hat{\mathbf{y}}$, at the expense of autonomy in time. The transformation is written as

$$\begin{aligned} t^* &= t \\ x^* &= x - \sigma y t \\ y^* &= y \\ z^* &= z \end{aligned}$$

to enter a set of quasi-Lagrangian coordinates which advect with the shear (*Barranco* 2006). Writing the differential operators explicitly,

$$\begin{aligned} \frac{\partial}{\partial t} &= \frac{\partial}{\partial t^*} - \sigma y^* \frac{\partial}{\partial x^*} \\ \frac{\partial}{\partial y} &= \frac{\partial}{\partial y^*} - \sigma t'^* \frac{\partial}{\partial x^*} \\ \nabla &= \nabla^* - \sigma t^* \frac{\partial}{\partial x^*}\hat{\mathbf{y}}, \end{aligned}$$

the Boussinesq equations can be transformed into shearing coordinates to obtain

$$\frac{\partial \boldsymbol{U}}{\partial t^*} - \sigma y^* \frac{\partial \boldsymbol{U}}{\partial x^*} = -(\boldsymbol{U}\cdot\nabla^*)\boldsymbol{U} + v\sigma t^* \frac{\partial \boldsymbol{U}}{\partial x^*} - \frac{\nabla^* p}{\rho_0} + \frac{\sigma t^*}{\rho_0}\frac{\partial p}{\partial x^*}\hat{\mathbf{y}} + \boldsymbol{U}\times f\hat{\mathbf{z}} - \frac{\rho}{\rho_0}g\hat{\mathbf{z}}$$

$$\nabla^*\cdot\boldsymbol{U} = \sigma t^* \frac{\partial v}{\partial x}$$

$$\frac{\partial \rho}{\partial t^*} - \sigma y^* \frac{\partial \rho}{\partial x^*} = -(\boldsymbol{U}\cdot\nabla^*)\rho + v\sigma t^* \frac{\partial \rho}{\partial x^*}.$$

Linearizing this system about the equilibrium solution $\bar{\boldsymbol{U}} = \sigma y^* \hat{\mathbf{x}}$, gives

$$\frac{\partial \boldsymbol{U'}}{\partial t'} - \cancel{\sigma y^* \frac{\partial \boldsymbol{U'}}{\partial x^*}} = \cancel{-(\bar{\boldsymbol{U}}\cdot\nabla^*)\boldsymbol{U'}} - (\boldsymbol{U'}\cdot\nabla^*)\bar{\boldsymbol{U}} - \frac{\nabla^* p'}{\rho_0} + \frac{\sigma t^*}{\rho_0}\frac{\partial p'}{\partial x^*}\hat{\mathbf{y}} + \boldsymbol{U'}\times f\hat{\mathbf{z}} - \frac{\rho'}{\rho_0}g\hat{\mathbf{z}}$$

$$\nabla^*\cdot\boldsymbol{U'} = \sigma t^* \frac{\partial \boldsymbol{v'}}{\partial x'}$$

$$\frac{\partial \rho'}{\partial t^*} = \cancel{\left(\sigma y^* - \bar{U}\right)\frac{\partial \rho'}{\partial x^*}} + w'\frac{\rho_0 N^2}{g}.$$

This system is now autonomous in x^*, y^*, and z^*, but not t^*. These normal modes are of the form

$$\xi = \hat{\xi}\,(t^*)\, e^{i(k_x x^* + k_y y^* + k_z z^*)}.$$

Writing the linearized system using this form of the field variables, it becomes

$$\begin{aligned}
\frac{d\hat{u}'}{dt^*} &= -\hat{v}'\sigma - ik_x\frac{\hat{p}'}{\rho_0} + f\hat{v}' \\
\frac{d\hat{v}'}{dt^*} &= -ik_y\frac{\hat{p}'}{\rho_0} + \frac{\sigma t^*}{\rho_0}ik_x\hat{p}' - f\hat{u}' \\
\frac{d\hat{w}'}{dt^*} &= -ik_z\frac{\hat{p}'}{\rho_0} - \frac{\hat{\rho}'}{\rho_0}g \\
ik_x\hat{u}' + ik_y\hat{v}' + ik_z\hat{w}' - ik_x\sigma t^*\hat{v}' &= 0 \\
\frac{d\hat{\rho}'}{dt^*} &= \hat{w}'\frac{\rho_0 N^2}{g}.
\end{aligned} \tag{14}$$

Now looking at the y-z plane, and setting $k_x = 0$, this system becomes autonomous in t^*. Writing the time derivatives as $-i\omega$, the system becomes purely algebraic,

$$\begin{aligned}
i\omega\hat{u}' &= \sigma\hat{v}' - f\hat{v}' \\
i\omega\hat{v}' &= ik_y\hat{p}'/\rho_0 + f\hat{u}' \\
i\omega\hat{w}' &= ik_z\hat{p}'/\rho_0 + \hat{\rho}'g/\rho_0 \\
k_y\hat{v}' + k_z\hat{w}' &= 0 \\
-i\omega\hat{\rho}' &= \hat{w}'\frac{\rho_0 N^2}{g}.
\end{aligned} \tag{15}$$

Setting the determinant of this homogenous system equal to 0 reveals the eigenvalue (or dispersion relation):

$$k_y^2 = k_z^2\frac{\left(\omega^2 - f^2 + \sigma f\right)}{N^2 - \omega^2} \tag{16}$$

or in terms of the angle θ between $\hat{\mathbf{y}}$ and $\boldsymbol{k}$,

$$\omega^2 = N^2\cos^2\theta + f\,(f-\sigma)\sin^2\theta.$$

Analyzing this result, it is apparent that waves can exist only if

$$N^2 > \omega^2 > f\,(f-\sigma)\,.$$

2.2 Variable $N(z)$, $k_x = 0$

Now allowing N to be a function of z, and staying in the shearing coordinates, the linearized system, 15, is reduced to being autonomous only in x^*, y^*, and t^* (if $k_x = 0$). The normal modes then look like

$$\xi = \hat{\xi}(z)\, e^{i(k_y y + k_z z - \omega t)}.$$

Writing the system using this functional form, it becomes

$$\begin{aligned} i\omega\hat{u}' &= \sigma\hat{v}' - f\hat{v}' \\ i\omega\hat{v}' &= ik_y\frac{\hat{p}'}{\rho_0} + f\hat{u}' \\ i\omega\hat{w}' &= \frac{1}{\rho_0}\frac{d\hat{p}'}{dz^*} + \frac{g}{\rho_0}\hat{\rho}' \\ ik_y\hat{v}' + \frac{d\hat{w}'}{dz^*} &= 0 \\ -i\omega\hat{\rho}' &= \frac{\rho_0}{g}N^2(z^*)\,\hat{w}' \end{aligned} \tag{17}$$

where the hatted field variables are all functions of z. The system can be rewritten as a single second order differential equation,

$$\frac{d\hat{w}'}{dz^{*2}} + k_y^2\frac{N^2(z^*) - \omega^2}{\omega^2 - f(f-\sigma)}\hat{w}' = 0.$$

Employing the WKB approximation given a slowly varying $N(z^*)$, and again defining

$$R^2(z^*) = k_y^2\frac{N^2(z^*) - \omega^2}{\omega^2 - f(f-\sigma)},$$

gives the approximate solution

$$\hat{w}' = \frac{A_0}{\sqrt{R}}e^{\pm i\int R dz}. \tag{18}$$

Analyzing the previous differential equation, it is apparent that a stable solution with $k_x = 0$ exists only for

$$N(z) > \omega > \sqrt{f(f-\sigma)}.$$

Since $R^{-\frac{1}{2}}$ is slowly varying (for $N \gg \omega$), by analogy with the result for constant N, (16), the z wavenumber becomes the term in the exponential. Noticing the same equivalence of terms as before it can be seen that, given $\frac{\omega}{N\sqrt{dN/dz}} \ll 1$, the dispersion relation is

$$k_z(z)^2 = k_y^2\frac{N^2(z) - \omega^2}{\omega^2 - f(f-\sigma)}. \tag{19}$$

In terms of θ, this becomes

$$\omega^2 = N^2(z)\cos^2\theta + f(f-\sigma)\sin^2\theta,$$

and the group velocity can be found as

$$\boldsymbol{c}_g = \frac{k_y k_z}{\omega k^4}\left[N^2(z) - f(f-\sigma)\right](k_z\hat{\mathbf{y}} - k_y\hat{\mathbf{z}}).$$

Again, the ray path can be traced analytically (since ω is found to be constant following the ray) by using the Eikonal set, (2), and the definition for the substantial derivative. Integrating the group velocity in time, the wave path becomes

$$y = \frac{\left[N^2(z) - \omega^2\right]}{\sqrt{\omega^2 - f(f-\sigma)}} \frac{\ln\left(N(z) + \sqrt{N^2(z) - \omega^2}\right)}{dN/dz} + c(z)$$
$$\text{where } c(z) = \frac{\ln\left(N(0) + \sqrt{N^2(0) - \omega^2}\right)}{dN/dz\sqrt{\omega^2 - f(f-\sigma)}} \left[N^2(z) - \omega^2\right].$$

Plotting the wave path in Figure 3, a cusp is seen where $N(z) = \Omega$. At that point, the solution

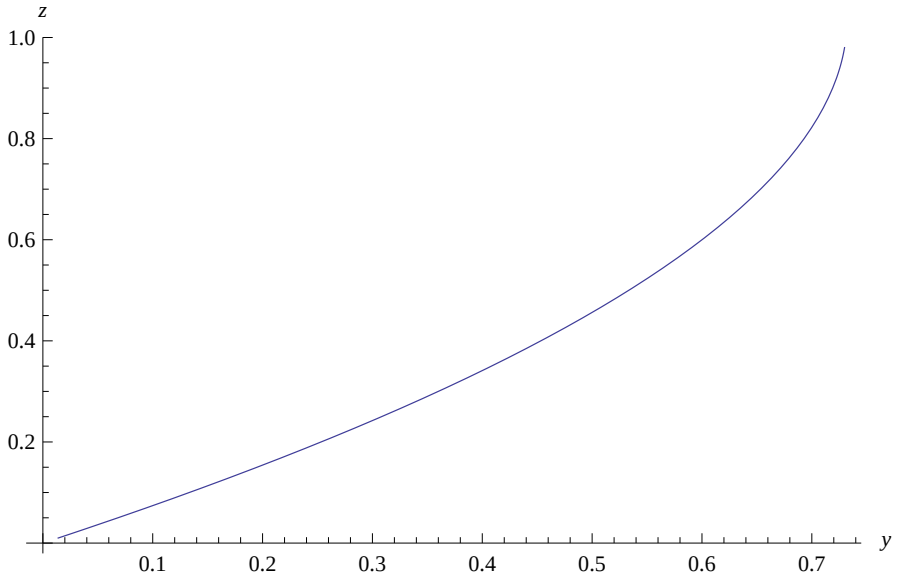

Figure 3: Analytical wave packet trajectory for variably stratified and shearing domain, $\omega = 2f = N_0 = 4\sigma$ and $N(z) = N_0(1 - z/5)$.

becomes purely imaginary and evanescent characteristics would be observed as the wave attempts to propagate in $\hat{\mathbf{z}}$. This reflection criterion can be implemented numerically, since for this analytical solution a wave energy balance is not accounted for in the governing equations. It should also be noted that although the y-z plane is the slice of interest, restricting the wave vector to this plane is an approximation and restricts an accurate evolution governed by the dispersion relation. To trace these paths for any given wavevector in $\Re^3$, a numerical method must be adapted.

3 Baroclinic Critical Layer

Now rescinding the assumption $k_x = 0$ as previously used, the governing equations are fully coupled to the Eikonal ray equations, and a numerical approach must be used. Solution of the Boussinesq set, (1), in Poloidal-Toroidal coordinates, where the cross-stream ($\hat{\mathbf{y}}$) direction is the poloidal ($\hat{\boldsymbol{\psi}}$) axis, gives a second order differential equation with variable coefficients. For succinctness it is kept

as a system of two equations written as

$$\begin{aligned}\Omega^2\hat{\boldsymbol{\psi}} &= \Omega\left(k_x\sigma - k_z f\right)\hat{\chi} + \frac{N^2}{k_\perp^2}k_x\left(k_x\hat{\boldsymbol{\psi}} - k_z\frac{d\hat{\chi}}{dy}\right)\\ \Omega^2\left(\frac{d^2\hat{\chi}}{dy^2} - k_\perp^2\hat{\chi}\right) &= fk_z\hat{\boldsymbol{\psi}}\Omega - \frac{N^2}{k_\perp^2}k_z\left(k_x\frac{d\hat{\boldsymbol{\psi}}}{dy} - k_z\frac{d^2\hat{\chi}}{dy^2}\right).\end{aligned} \tag{20}$$

It is well known that critical layers exist at locations where the coefficient of the highest (second) order term is zero. Solving for the locations of the Baroclinic critical layers (*Marcus*, 2013) gives

$$y^* = \frac{\omega \pm N}{\sigma k_x}, \tag{21}$$

where y^* is a displacement quantity from the location of the perturbation.

3.1 Numerical Method

The Boussinesq equations linearized about $\bar{\boldsymbol{U}} = \sigma y\hat{\mathbf{x}}$ are again given by system 12. Utilizing the method of multiple time scales, spatial quantities are decomposed into slowly varying, (X, Y, Z), and fluctuating, (x, y, z) terms. Although this system is not autonomous in y or z, it can be locally approximated as such for a small enough range, $y - \delta \leq y \leq y + \delta$, and similarly in z. Thus the normal modes are locally approximated as

$$\xi = \bar{\hat{\xi}}\left(Y, Z\right)e^{i(k_x x + k_y y + k_z z - \omega t)}$$

where the coefficient has been split into a slowly varying function of $Y$and Z, $\bar{\hat{\xi}}$, and a quickly varying, oscillatory function of y and z, $e^{i(k_y y + k_z z)}$. For small length scales, such that $\delta \ll k^{-1}$, the differential operators relating the two scales can be represented as

$$\frac{\partial}{\partial \boldsymbol{x}} = \epsilon\frac{\partial}{\partial \boldsymbol{X}}.$$

This notation allows the spatial derivatives of the normal modes to be written as

$$\frac{\partial \xi}{\partial y} = \epsilon\frac{d\bar{\hat{\xi}}}{dy}e^{i(\boldsymbol{k}\cdot\boldsymbol{x} - \omega t)} + ik_y\bar{\hat{\xi}}e^{i(\boldsymbol{k}\cdot\boldsymbol{x} - \omega t)}$$

and similarly for the partial derivative in terms of z. Rewriting the linearized Boussinesq set using the normal modes, and omitting terms of order ϵ or higher, the system becomes

$$\begin{aligned} i\omega\hat{u}' &= ik_x\bar{u}\hat{u}' + \frac{ik_x}{\rho_0}\hat{p}' - \hat{v}'f\\ i\omega\hat{v}' &= ik_x\bar{U}\hat{v}' + \hat{u}'f + \frac{1}{\rho_0}ik_y\hat{p}'\\ i\omega\hat{w}' &= ik_x\bar{U}\hat{w}' + \frac{ik_z}{\rho_0}\hat{p}' + \frac{\hat{\rho}'}{\rho_0}g\\ ik_x\hat{u}' + ik_y\hat{v}' + ik_z\hat{w}' &= 0\\ i\omega\hat{\rho}' &= ik_x\bar{U}\hat{\rho}' - \hat{w}'\frac{\rho_0 N^2}{g}.\end{aligned} \tag{22}$$

By eliminating first order small terms, an analytically insoluble coupled second order differential equation with variable coefficients has become an algebraic system which is valid for local values of y and z, with error scaling linearly with ϵ. Defining $\Omega \equiv \omega - \bar{U}k_x$ as the extrinsic frequency, this system of equations is solved to give the complex-valued dispersion relation,

$$\left(\Omega^2 - N^2\right)\left(\Omega k_x^2 - i\sigma k_x k_y + \Omega k_y^2\right) + \Omega\left(\Omega^2 - f\left(f - \sigma\right)\right)k_z^2 = 0. \tag{23}$$

This relationship is summarized as $\omega = \mathcal{W}(y, z, k_x, k_y, k_z)$. It can be shown that when either $\sigma = 0$ or $k_x = 0$ this reduces down to the previous dispersion relations derived in Sections 1 and 2 respectively. Also note that for slowly varying shear in $\hat{\mathbf{y}}$, corresponding to ϵY, this dispersion relation approaches the real-valued limit (*Jones*, 1969).

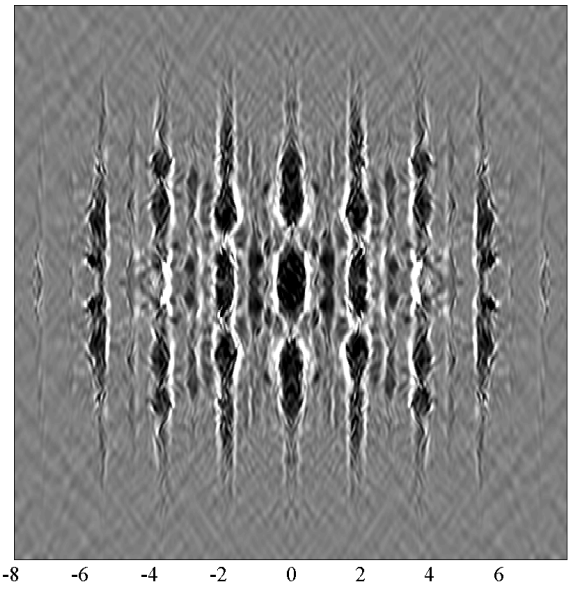

Figure 4: Vertical vorticity, ω_z, shown in grayscale of a radial slice revealing a lattice of *Zombie Vortices*. Anticyclonic vorticity is shown in black and cyclonic in white.

With knowledge of the dispersion relationship the ray equations can be aptly simplified. Writing the total derivative of ω, and using the Eikonal relations, 2, it is apparent that $\omega = \omega_0$ is constant following a ray. Additionally, since there is no explicit x dependence in the dispersion relation, $k_x = k_{x,0}$ is similarly constant along a ray. The equations describing the wave evolution then look like

$$\begin{aligned} \frac{dk_y}{dt} = -k_x\frac{\partial U}{\partial y} - \frac{\partial \Omega}{\partial y} &= -k_x\sigma \\ \frac{dk_z}{dt} &= -\frac{\partial \Omega}{\partial z} \\ \frac{dx}{dt} = c_{g,x} + \bar{U}_x &= \frac{\partial \omega}{\partial k_x} + \sigma y \end{aligned} \tag{24}$$

By inspection of these evolution equations, it is seen that while following the ray, k_y evolves linearly in time. Additionally, the velocity of the wave packet is simply the vector sum of the shear velocity and group velocity. Rewriting the complex dispersion relation, (23), as a cubic in terms of the extrinsic frequency, Ω, it becomes apparent that three solutions exist. Whereas the one root is purely

imaginary, the other two roots are complex and will trace out waves traveling with components in the $\pm\hat{\mathbf{y}}$ directions. To verify with the pseudospectral fluid simulations which show the presence of zero frequency arms, a ray must be traced with $\omega = 0^+$. The three solutions of the complex dispersion relation then consist of a trivial solution, and two for which $k_z^2 = \frac{N_0^2 k_x^2}{f(f-\sigma)}$, (upward- and downward-propagating), corresponding to the extraordinary and ordinary rays, respectively. Using these three solutions along with (24) gives a fully determined system describing the *local* evolution of the ray. An iterative, adaptive 5th order Runge-Kutta numerical scheme was used to integrate these equations along the complex ray path, at each point satisfying the dispersion relation which consequently necessitates the propagation direction. Finally, the energy evolution of the wave packet can be found by interpreting the imaginary term of the wavevector as a decaying amplitude. Writing the nondimensional energy change, as $E^* = \frac{E}{E_0} = \int_p e^{-(\boldsymbol{x}\cdot \mathrm{Im}(\boldsymbol{k}))} d\boldsymbol{x}$, the wave evanescence becomes evident. Further discussion of the implications and interpretations of these complex-valued field variables follows in Section 3.2.

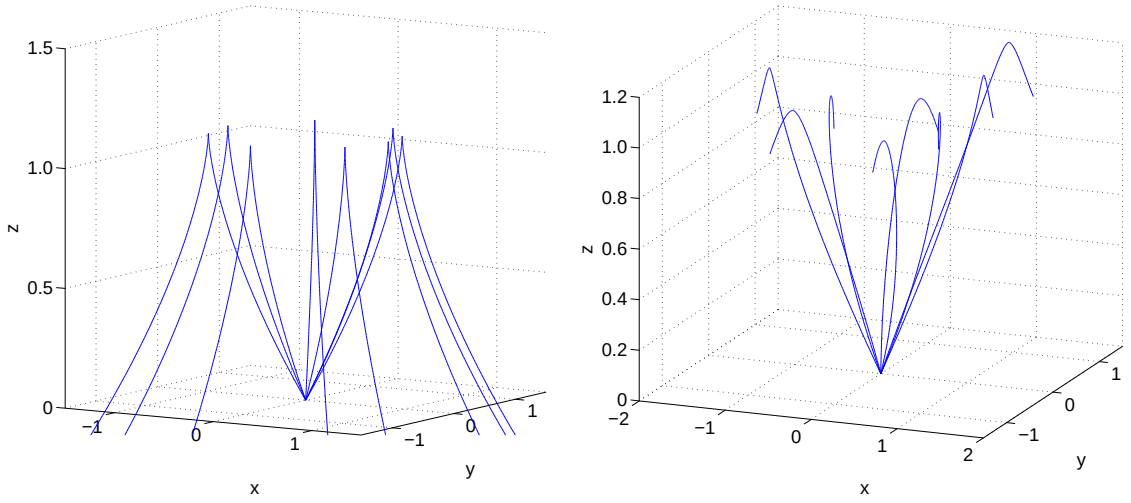

(a) Evanescent wave reflection off of density stratification layer, where $N(z=1) = \omega$.

(b) Wave reflection with shear.

Figure 5: Wave reflection and profile of continuously stratified, rotating medium, with and without shear. Test case for $\sigma \to 0$, showing continuity of Complex- and Real-valued Ray Tracing methods.

The simplest test case used to verify this code was to force $k_x \neq 0$ waves by setting $N = \sqrt{f(f-\sigma)}$. Imposing this condition, along with the now overdetermining definition for k_x, gives consistent results for both $k_x \neq 0$ and the run of interest, $k_x = 0$. Setting both $k_x = 0$ and imposing the condition for N contradicts each other and a purely imaginary, evanescent result is obtained, in agreement with the analytical case given in Section 2.2. A second limiting test case was used to ensure agreement between the complex- and real-valued dispersion relations as $\sigma \to 0$. These cases are presented in Figure 5. Note the absence of a cusp in the test case presented in Figure 5(b). This can be explained by noticing that the group velocity in the x-y plane nearly drops to zero, allowing the shear to smooth out the discontinuity where $N(z) = \omega$ seen in the y-z plane. The consistency of the code was also confirmed by ensuring local satisfaction of the Dispersion Relation, which agrees to within working precision when allowing complex-valued variables.

3.2 Complex Wavevector Interpretation

Given the less than physical nature of a complex ray equation and path integrals along a complex path, the following is included to help rectify these concerns.

Since it is known that $\{N, \omega, \sigma, f, k_x\} \in \Re$ by construction, and the dispersion relation is allowed to be a complex function, the y and z wavenumbers then must exist in complex space. The complex-valued wavevectors can be interpreted as producing a decay term, much as an evanescent wave has a purely imaginary wavevector (*Shaman*, 2012). These waves then could be considered "semi-evanescent" or "quasi-caustic", specifically when propagating with components in the $\hat{\mathbf{y}}$ or $\hat{\mathbf{z}}$ directions.

Allowing complex-valued ray paths has another important ramification. Specifying an initial perturbation frequency, ω_0, and horizontal wavevector, $\mathbf{k}_\perp = k_x\hat{\mathbf{x}} + k_y\hat{\mathbf{y}}$ is not enough to determine the group velocity. Since the complex dispersion relation, Equation 23, is a cubic in Ω, there are then three possible ray path solutions. Two of these roots correspond to ordinary rays, which obey refraction laws in $\Re$, whereas the other one is termed an extraordinary wave. The solution to the extraordinary ray does not refract as one is used to in physical space (Snell's Law), since the imaginary part of the wavevector is orders of magnitude larger than for the ordinary rays. This solution still obeys the dispersion relation, however, due to the presence of the imaginary components of $\mathbf{k}$. The imaginary components effectively act as an implicit property of the wave, despite its non-physical characteristics.

4 Results

The linear pseudo-spectral fluids simulation is mapped on the surface plot in Figure 6, with each of the complex and real ray paths plotted on top, revealing the zero-frequency arms reaching towards the Baroclinic critical layers. Note that a composite plot from two simulations is shown: One with an $m = 1$ wave generator located along the x-axis, and the second with $m = 2$. Consistency in the complex ray tracing method can also be seen by comparing each ray to the approximated real ray. For these parameters, chosen to match a Keplerian disk, the shear ($\sigma = \frac{3}{2}\Omega_\odot$) is not large enough for the imaginary term to greatly affect the ray, making spatial corrections $< 5\%$ relative to the real ray.

The complex ray tracing results follow the path of the zero frequency numerical simulation arms, although because the dispersion relation does not consider non-linear effects, deviations between the wave packet and energy path are observed for the linearly stratified domain. Remnant internal intertia-gravity waves can be seen past the sixth generation of critical layers where they are beginning to instigate the next generation of vortices. This fully non-linear and anelastic simulation differs from the idealized results shown in Figure 6 obtained using a wave generator of a single frequency.

As the wave packet evolves in time, the imaginary shearing term causes the wavevector to take on complex values. For positive imaginary components of $\mathbf{k}$ as well as shear, this is analogous to a spatial decay term, evidenced by writing the eigenmodes explicitly, and noting the wave acts as if it is becoming evanescent in the shear. Alternatively, when the wavevector supplements the dispersion relation (the imaginary part is negative) the wave draws energy from the background flow, and the previous analogy breaks down. Thus, complex rays can have caustics (but don't necessarily reflect), just like real rays are evanescent.

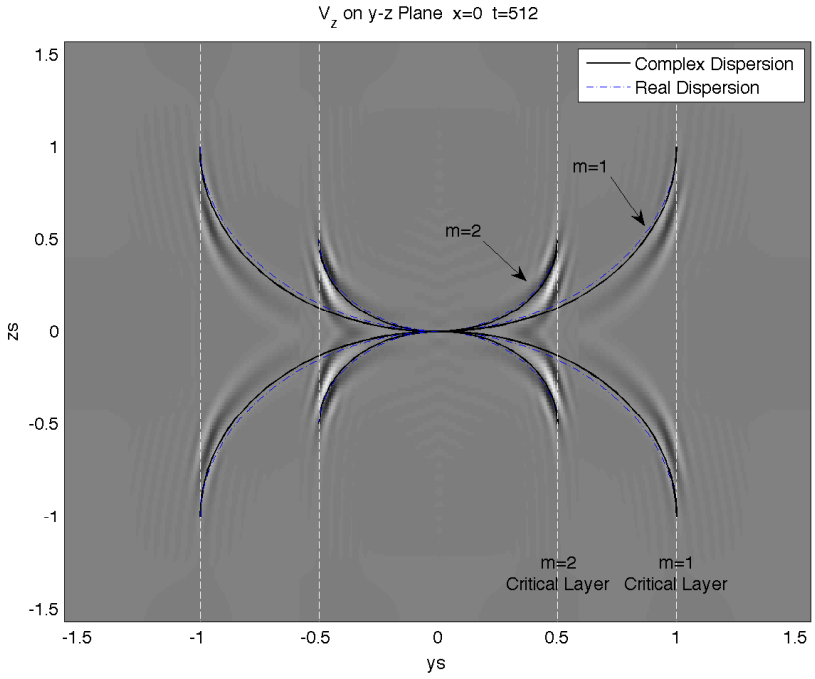

Figure 6: Hybrid overlay of numerical Ray Tracing path on spectral simulations with constant N, $\omega = 0$.

By tracking the energy evolution, it was found that these quasi-caustic waves draw or lose energy from the background shear, depending on whether the wave is propagating into the shear or with it, respectively. In the case for Figure 7, the wave packet is traveling in the $+\hat{\mathbf{x}}$ direction, and thus loses energy to the background shear. Unlike the case with no shear, the wave action—a quantity many recognize as conserved, $\mathcal{A} = E/\Omega$—is not constant in a shearing domain. As the wave packet propagates and nears the critical layer, the group velocity slows, and the energy is found to accumulate there. It is this local spike in energy that exceeds the threshold and instigates the next generation of the instability, seeding another vortex at subsequent critical layers as evidenced in Figure 4.

The impact the imaginary wavenumber term has on the dispersion relation can be elucidated by noting that the real dispersion relation is not satisfied, with the difference being $\mathcal{O}(\sigma \mathrm{Im}(k_y))$ relative to the real part of the complex dispersion relation. Thus, the complex wavevectors carry implicit information about the wave packet refraction behavior in the flow, which is expressed when k_y evolves to be largely imaginary.

A critical layer in shearing flow can also exist with asymptotic reflections off of the shear, rather than cusp reflections off of the density stratification. This critical layer appears where the extrinsic frequency tends to zero, equivalently, where $k_x \sigma y^* = \omega_0$. These critical layers are impossible in still background conditions since $\Omega = \omega_0$ is constant throughout. This agrees with the results for the Baroclinic critical layers, giving Equation 21: As $\sigma \to 0$, $y^* \to \infty$ and no critical layer exists.

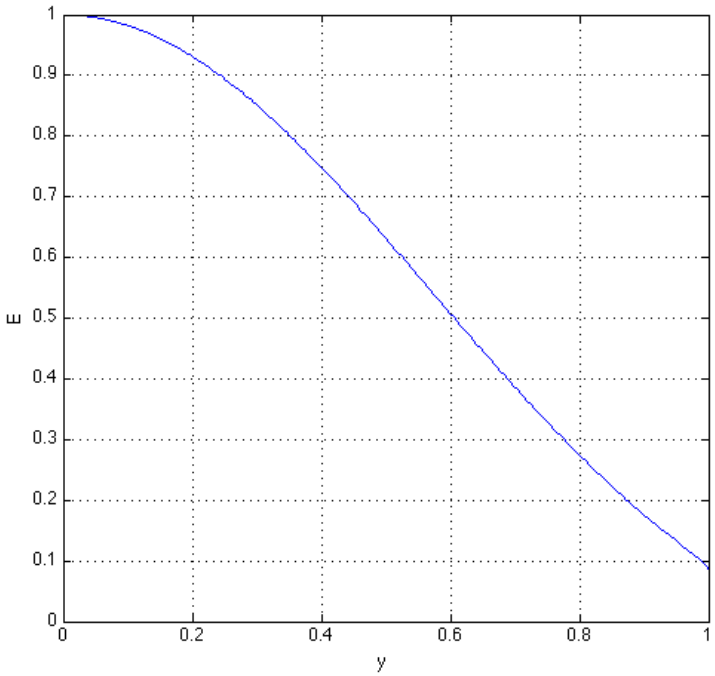

Figure 7: Energy evolution in time, Linear $N(z) = N_0(1 - z/2)$, $k_x = 1$, $\omega = 0^+$.

5 Conclusion

A complex Eikonal ray tracing method has been presented and shown to be consistent with spectral shearing sheet simulations in a stratified, shearing, and rotating domain. It was also shown that for the presented problem set up, little variation is found between tracing a complex and real path, likely due to the relative Keplerian shearing rate used.

Regardless of the proposed complex ray tracing methods, both simulations support the conclusion that the phenomena in the spectral simulations are ordinary rays whose energy, and information extend between vortices in the lattice, providing a sufficient self-sustaining perturbation. Future work will explore the nonlinear effects on these gravity waves by comparing with internal gravity waves originating from a seed vortex.

(Other applications? Ray tracing in the atmosphere. Where else are Eikonal Equations projected onto the real plane as an approximation?)

References

[1] Dave Broutman, James W. Rottman, and Stephen D. Eckermann. Ray Methods for Internal Waves in the Atmosphere and Ocean. *Annual Review of Fluid Mechanics*, 36(1):233–253, January 2004.

[2] W. Dieminger, G. K. Hartmann, and R. Leitinger. Investigation Methods of the Upper Atmosphere. In *The Upper Atmosphere*, pages 203–399. 1996.

[3] Louis Gostiaux, Denis Martinand, and Thierry Dauxois. Experiments on Reflection of Internal Gravity Waves : Without and With Rotation. Technical report, 2004.

[4] Frank S Henyey, J O N Wright, and Stanley M Flattl. Energy and Action Flow through the Eikonal Wave Field. *Journal of Geophysical Research*, 91(C7):8487–8495, 1986.

[5] Chung-Hsiang Jiang and Philip Marcus. *Selection Rules for the Nonlinear Interactions of Internal Gravity Waves and Inertia-Gravity Waves*. PhD thesis, 2010.

[6] Walter L Jones. Ray Tracing for Internal Gravity Waves. *Journal of Geophysical Research*, 74(8), 1969.

[7] M. V. Kalashnik. Propagation and Trapping of Inertial Gravity Waves in Shear Flows (Ray Theory). *Izvestiya, Atmospheric and Oceanic Physics*, 49(2):217–228, April 2013.

[8] P K Kundu and I M Cohen. *Fluid Mechanics, Volume 10*. 2008.

[9] E Kunze. Near-Inertial Wave Propagation in Geostrophic Shear. *Journal of Physical Oceanography*, 15:544–556, 1985.

[10] James Lighthill. *Waves In Fluids*. 1978.

[11] Philip S Marcus, Suyang Pei, Chung-hsiang Jiang, and Pedram Hassanzadeh. Self-Replicating Three-Dimensional Vortices in Neutrally-Stable Stratified Rotating Shear Flows. 2013.

[12] R. Mied and J. Dugan. Internal Gravity Wave Reflection by a Layered Density Anomaly. Technical Report 7, 1974.

[13] F. Y. Moulin and J.-B. Flór. VortexWave interaction in a Rotating Stratified fluid: WKB Simulations. *Journal of Fluid Mechanics*, 563:199, September 2006.

[14] Dirk Olbers. The Propagation of Internal Waves in a Geostrophic Current. *Journal of Physical Oceanography*, 1:1224–1233, 1981.

[15] K. Peat. Internal and Inertial Waves in a Viscous Rotating Stratified Fluid. *Applied Science Research*, 33(1):481–499, 1978.

[16] A. Satyanaryanan and P. L. Savhdev. Reflection of Internal Gravity Waves in an Atmosphere with Wind Shear: WKB Approximation. *Journal of Pure Applied Math*, 11(12):1696–1703, 1980.

[17] Jeffrey Shaman, R. M. Samelson, and Eli Tziperman. Complex Wavenumber Rossby Wave Ray Tracing. *Journal of the Atmospheric Sciences*, 69(7):2112–2133, July 2012.

[18] Stefan G Llewellyn Smith. Generation of Internal Gravity Waves by an Oscillating Horizontal Elliptical Plate. *Journal of Applied Mathematics*, 72(3):725–739, 2012.

[19] C Staquet and J Sommeria. Internal Gravity Waves : From Instabilities to Turbulence. *Annual Review of Fluid Mechanics*, 34:559–593, 2002.

[20] Bruce R Sutherland. *Internal Gravity Waves*. 2010.

[21] Steven Weinberg. Eikonal Method in Magnetohydrodynamics. *The Physical Review*, 126(6):1899–1909, 1962.